IOSR Journal of Pharmacy and Biological Sciences (IOSR-JPBS)
e-ISSN: 2278-3008, p-ISSN:2319-7676. Volume 9, Issue 1 Ver. VI (Feb. 2014), PP 77-85
www.iosrjournals.org

Synthesis and In Vitro Antibacterial Properties of Hydroxyapatite Nanoparticles

H. S. Ragab[1], F. A. Ibrahim[1], F. Abdallah[1], Attieh A. Al-Ghamdi[2], Farid El-Tantawy[3], Neyara Radwan[3,] F. Yakuphanoglu[4]

[1]*Department of Physics, Faculty of Education, Suez Canal University, El-Arish, Egypt*
[2]*Department of Physics, Faculty of Sciences, King Abdulaziz University, North Campus, Jeddah, Saudi Arabia*
[3]*Department of Physics, Faculty of Science, Suez Canal University, Ismailia, Egypt*
3 Mechanical Department, Faculty of Engineering, Suez Canal University, Ismailia, Egypt
[4]*Department of Physics, Faculty of Science, Firat University, Elazig, Turkey*

Abstract: *hydroxyapatite (HAP, $Ca_{10}(PO_4)_6(OH)_2$) nanoparticles are important biocompatible materials and were successfully synthesized by a new and simple precipitation process using calcium hydroxide, phosphoric acid as phosphorus (P) and calcium (Ca) precursors and sodium hydroxide (NaOH). The crystal structures and morphologies of the as synthesized hydroxyapatite were analyzed by X-ray diffractions (X-ray), Fourier transform infrared spectroscopy (FTIR), field emission scanning electron microscopy (FESEM), energy dispersive x-ray spectroscopy (EDS) and transmission electron microscopy (TEM). Single phase HAP, with an average grain size of about 19 nm and surface area of 61 m^2/g, was obtained. Additionally, the antibacterial activity of the as synthesized HAP nanoparticles related to gram positive and gram negative bacteria's were examined, too. Finally, the obtained results indicated that the HAP nanoparticles possess excellent and a broad spectrum antibacterial activity and it can potentially be applied in medical and environmental fields.*
Key Words: *hydroxyapatite nanoparticles, microstructure, antibacterial activity*

I. Introduction

The biotechnology for repairing bone is vital in our lives and in an aging society, because the bone tissue becomes weak with age and elderly people often suffer from trauma and damage to the bone tissue hence their damages induces the significant decrease in the quality of our life [1-3]. In fact, many common materials like metals/alloys and polymers composites have been intensively applied in biotechnology to bone repair damaged parts of the body and substitution [4,5]. Unfortunately, metals and its alloys are suffer from disadvantage properties like easy corrosion and not tailored mechanical characteristics (i.e. high mechanical strength and stiffness) compared to true bone [6]. The development in modern medical science has improved biomaterials role in replacing damaged tissue, organs, and improving their functions. Hydroxyapatite (HAP) one of the apatite minerals with a chemical formula of ($Ca_{10}(PO_4)_6(OH)_2$), is a major inorganic constituent about 60-70 % of the inorganic portion of the bone matrix and possesses the high ability of ion-exchange against various cations which make that HAP has high biocompatibility and bioactivity properties [7-10]. Besides HAP can be used in a wide range of applications such as bone substitution, fertilizers, food supplements as a source of calcium, dental materials, drug delivery agent, gene carriers biology, adsorbent of liquid chromatography and proteins, catalysts, ion exchangers, removal of organic pollutants like phenol and other divalent metal cations, gas sensors, proton conductors and more [4,5]. However, bacterial contamination caused by adhesion and colonization on biomaterials surface is an important post-implantation problem and a considered complication of traumatology and orthopedics. Thus, the antibacterial properties of metal oxides nanoparticles such as ZnO, MgO, TiO_2, CeO_2, etc are important for promising medical and environmental applications. The subject of this work is to synthesized hydroxyapatite nanoparticles via new and simple precipitation chemical process using a $Ca(OH)_2$, orthophosphoric acid (H_3PO_4) and sodium hydroxide (NaOH) to adjust pH value for the first time. The microstructures of as prepared hydroxyapatite nanoparticles were examined in details. Finally, the applicability of as prepared hydroxyapatite nanoparticles toward several gram positive and gram negative bacterial was tested, too. It proved that HAP nanoparticles can potentially be applied in medical and environmental fields.

II. Experimental Details

2.1 Preparation of Hydroxyapatite Nanoparticles

All the reagents used in this experiment were analytically pure and were received from commercial sources. All the chemicals were used without further purification. In a typical synthesis, 10.9 gm (1.11 M) orthophosphoric acid (H_3PO_4) was dropwise added into 11.1gm (1.5 M) calcium hydroxide $Ca(OH)_2$ solution under strong magnetic stirring at 70 ^{0}C for 3 h till the molar ratio of Ca to P rose to 1.67. The mixture was

stirred until a clear and homogeneous solution formed, and 2 mol of NaOH was added dropwise to this solution until pH value maintained to be 10. The white precipitate HAP gel was precipitated after aging for 4 h. The obtained HAP solid products were separated, washed repeatedly with de-ionized water, and dried under ambient atmosphere. The yield of HAP nanoparticles was up to almost 100%. The solid products were then heated in an electric furnace at 700 ^{0}C for 1 h in air, and final products were obtained.

2.2 Characterization

X-ray diffraction (X-ray) patterns were obtained by an X-ray diffractometer (D/max-2200/PC, Rigaku Corporation, Japan) with $Cuk\alpha$ $(\lambda = 0.15406\ nm)$ radiation. The working conditions were 40 kV and 30 mA for the X-ray tube, scan speed 0.041, and 2s measuring time per step. Infrared spectra of the samples were performed with Nicolet Avatar Model FTIR spectrometer using KBr discs in the range 400 - 4000 cm^{-1}. Morphology and structural features of as prepared hydroxyapatite nanoparticles were analyzed by both scanning and transmission electron microscopy. Field emission scanning electron microscope (FESEM) measurements were conducted on JEOL 2010 with an accelerating voltage of 10 kV. Transmission electron microscope (TEM) and high-resolution transmission electron microscope (HRTEM) measurements were performed on a JEM-2100F (JEOL Ltd.) with an accelerating voltage of 200 kV.

2.3 Antibacterial activities in solid agar medium

This test was carried out according to the method of Joshi *et al*., in 2009, which was performed in sterile Petri-dishes with 90 mm diameter containing sterile Nutrient agar medium (15 ml). After the renewal of cultures bacterial for 24 h., the freshly prepared bacterial inoculums was swabbed over the entire surface of the medium three times, rotating the plate 60 degrees after each application by using sterile cotton swab, to ensure the spread of bacteria on the surface of the plates. One well of 6mm diameter was bored in the medium for each plates with the help of sterile cork-borer and was filled with 50 µl of the suspension of the tested material using micropipette. , Ampicilin (5µg/ml) was used as positive control and water was used as negative control. Plates were left for 45 min at room temperature to allow proper diffusion of the extract to occur in the medium. All plates were incubated at 37°C for 24 h, followed by the measurement of the diameters of zones of inhibition. Inhibition of bacterial growth was measured as zone diameters (mm) at 3-equidistant points taken from the centre of the inhibition zone, and the average value was taken. All experiments were carried out in triplicate and the reported data represents average values ±SD.

2.4 Antibacterial activities in liquid medium

Different concentrations of the tested material were prepared and added to 48 ml of nutrient broth medium in 250 ml Erlenmeyer flasks to give 100 to 900 µg/ml). Each flask was inoculated with 2 ml of the tested bacterium containing 5x10^5/ml and the flasks were incubated at 37^{0}C. The bacterial growth was determined by measuring the absorbance at 595 nm. Control flasks without nanomaterial were prepared as control.

2.5 Mode of action of the tested nanomaterials

After incubation of the tested bacterium in nutrient broth medium containing different concentrations of the MO and ZnO ranging from 100-900 µg/ml, bacterial cells were collected by centrifugation at 3000 rpm and were washed several times with sterile distilled water. The collected cells were resuspended in sterile distilled water (OD. at 550 = 0.65). Cell respiration (quantity of O_2 consumed/min was determined using Oxigraphe. The quantity of K^+ flowed from the treated and untreated cells were determined using atomic adsorption (Aly , 1997).

III. Results and Discussion

3.1 Structural Properties of HAP nanoparticles

The crystallinity and crystal phases of the as-synthesized HAP nanostructures were examined by powder X-ray diffraction. The typical X-ray patterns of the as synthesized hydroxyapatite nanostructure is depicted in Fig. (1). Obviously, all diffraction peaks in this pattern can be indexed to the well-crystallized single phase hydroxyapatite and consistent with the reported literature [2,3]. No other reflections other than HAP reflections, related to any impurity are detected in the pattern which verifies that the synthesized nanoparticles are pure hexagonal phase hydroxyapatite.

The average crystallite size (D) of the prepared HAP was calculated from the Scherrer relation [1,2]:

$$D = \frac{0.91\lambda}{\beta_{1/2}\cos\theta} \qquad (1)$$

The degree of crystallinity (X_c) was calculated using following equation [2]:

$$X_c = \left(\frac{K_c}{\beta_{1/2}} \right) \quad (2)$$

The surface area (S) estimated using the following empirical formula [3]:

$$S = \frac{6}{D\rho} \quad (3)$$

where λ is the wavelength of the X-ray used $(\lambda = 0.15406\ nm)$, θ is the diffraction angle in degrees (002) and ((211), $\beta_{1/2}$ is the full width at half maximum (FWHM) of the (002) x –ray reflection (in degrees), K_c is a constant set at 0.24, and ρ is the density of the prepared HAP and measured using Archimedes technique [4].

The crystallite size of the synthesized HAP is estimated to be about 19 nm, with crystallinity about 87 % and surface area about 61 m^2/g.

The lattice constants of $a-axis$ and $c-axis$ of the HAP were calculated from peak (002) using the equation belonging to hexagonal system [4]:

$$\frac{1}{d^2} = \frac{4}{3}\left(\frac{h^2 + hk + k^2}{a^2} \right) + \frac{l^2}{c^2} \quad (4)$$

where d is the distance between two adjacent planes, h, k and l are the Miller indices and a and c are the lattice constants of the unit cell.

The volume (V) of unit cell was calculated using the following equation [7]:

$$V = \frac{\sqrt{3}}{2} a^2 c \quad (5)$$

The calculated lattice constants of as prepared HAP are a= 0.941 nm, c=0.685 nm and $V = 0.5196\ nm^3$. These lattice parameters were similar to the data listed in JCPDS (PDF No.09-0432).

For the detailed functional groups and compositions present, the synthesized HAP nanoparticles were examined by Fourier transform infrared (FTIR) spectroscopy. FTIR spectra of the as prepared HAP nanoparticles are depicted in Fig. (2). It is clear that the broad band at 3569 cm-1 arise from hydroxyl stretching and librational modes of OH^- due to the presence of an organized water structure in HAP and/or hydrated layer along with HAP. The carbonate band CO_3^{2-} of impurity ion appears at 1420 cm^{-1} due to the sample preparation in the atmosphere, which leads to dissolve CO_3^{2-} to carbonate that replace PO_4^{3-} ion in HAP lattice. Also, the band appears at 1463 cm^{-1} according to replace OH^{-1} ions in HAP lattice. The presence of three distinct bands at 469, 603 and 964 cm-1 are due to symmetric metal - oxygen $P-O$ stretching vibration of PO_4^{3-} which confirm the formation of hexagonal hydroxyapatite. In addition to this an absorption bands appeared at 1033 and 1097 cm-1 is attributed to asymmetric stretching modes. In conclusion, it is interesting to note that the sharp peaks belonging to the hydroxyl and phosphate groups in FTIR spectrum of HAP sample support the well-crystallized apatite structure and all bands in FTIR spectra showed the typical bands of HAP [5,6].

To investigate the general morphologies of as-synthesized spherical-shaped hydroxyapatite nanostructures, the synthesized products are examined by FESEM and demonstrated in Fig. (3 a,b). From the obtained FESEM micrographs, it is clear that the synthesized products are uniform size and highly aggregated which are formed in large-quantity. Furthermore, The FESEM images showed spherical - like morphology with average diameter of 19 nm. It is worthily to note that the microstructure of HAP is very similar to that of the natural bone.

Again, to check the composition of as-synthesized HAP nanoparticles, energy dispersive spectroscopy (EDS) was performed and demonstrated in Fig. (3c). The EDS result indicated that the as synthesized HAP

nanoparticles were composed of Ca, P and O only. No other peaks related to any impurity are detected in the EDS spectrum, up to the detection limit of EDS instrument and thus, again confirms that the synthesized products are pure HAP made of Ca, P and O. Semiquantitative analysis indicates that the Ca/P molar ratio is about 1.66 and it is closer to the theoretical value of 1.66, confirming that the nanoparticles are hydroxyapatite. The peak corresponding to C comes from the SEM substrate.

The size and morphology of the prepared HAP nanostructures were determined by TEM observations. Low – resolution TEM images and the selected area diffraction (SAED) pattern of synthesized HAP nanoparticle are depicted in Fig. (4a,b), respectively .The image of the HAP showed spherical-like morphology with average diameter of 19 nm. Furthermore, the TEM image showed high aggregates of spherical rice grain like nanostructures with average diameter of 18 nm, which show full consistency with the observed FESEM results. Fig. (4b) confirms that the SAED patterns of the above samples exhibit diffraction rings rather than individual spots indicating the polycrystalline nature of the samples. Fig. 4 (c) demonstrates the typical high-resolution TEM image which exhibits clear and well-defined lattice fringes of the synthesized hydroxyapatite nanoparticles. The measured spacing between two lattice fringes are 0.2815 nm which corresponds to the (211) plane of hexagonal hydroxyapatite. The well-defined lattice fringes again confirmed that the synthesized HAP nanoparticles possessing well-crystalline structures as confirmed above.

3.3 Antibacterial Activity of HAP Nanoparticles

The antimicrobial activity tests were performed against the bacteria E. coli and Bacillus sp. The dependence of bacterial growth on the concentration $(G-C)$ of the prepared HAP spherical nanoparticles is depicted in Fig. (5). It is clear that the bacterial growth decreases rapidly and exponentially with increasing HAP nanoparticles concentration up to certain concentration of about 700 mg/l and then slightly decreases. Noteworthy, the E. coli bacteria has a rapid bacterial growth compared to Bacillus sp bacteria. This implies that the HAP nanoparticles have higher bacterial efficacy against E. coli. There are several reasons to explain the different results of the antibacterial tests for E. coli and Bacillus sp. First, the cell wall attributes differ between Gram-positive bacteria (Bacillus sp) and Gram-negative (E. coli). Normally, E. coli has a relatively thin cell wall made of peptidoglycans and lipopolysaccharide. Second, Bacillus sp., has a thick cell wall, consisting of a large amount of mucopeptides, murein and lipoteichoic acids (immunostimulator molecule). Furthermore, the golden carotenoid pigments and the antioxidant enzymes (catalase) of Bacillus sp. give this bacteria a bit stronger oxidant resistance. Additionally, cell-wall properties, like cell permeability and capability of solubilizing HAP entire bacteria might also be considered [8].

However, the bacterial growth – concentration $(G-C)$ curve in Fig. (5) can be described by an exponential decay equation as:

$$(G-G_m)=(G_m-G_0)(1-\exp-(C/C_t)) \qquad (5)$$

where G_m and G_0 are the maximum and initial bacterial growths and C_t is the exponential decay concentration constant and strongly depends on HAP concentration and is calculated as $C=C_t$.

The computed values of C_t as a function of HAP concentration is about 422 and 613 gm/l for E. coli and Bacillus sp. bacteria, respectively. It is interesting to mention that the value of C_t for E. coli is less than Bacillus sp. This strong clue supporting that the HAP nanoparticles has higher antimicrobial efficacy towards E. coli bacteria. Therefore, we recommend using these HAP nanoparticles as antibacterial agent for E. coli and can potentially be applied in medical and environmental fields.

To confirm the above facts, we screened the scanning electron microscopy (SEM) of normal cell of E. coli in nutrient broth medium after 24 h of growth at 37 ^{0}C and treated cells of E. coli supplements with 0.7 g/l HAP nanoparticles as depicted in Fig. (6 a,b), respectively. It is clear that treatment of the E. coli bacteria with HAP nanoparticles has led to considerable damage to E. coli which caused the breakdown of the bacterial cell wall [9]. In addition, because particle size of HAP is about 19 nm, the aggregation effect becomes very significant due to the high surface area of the synthesized HAP nanoparticles which is about 52 m^2/g. Thereby, the HAP nanoparticles activate the bacterial grovel and spores so that bactericidal efficiency becomes higher. Furthermore, the inhibition of bacterial growth for cell wall is attributed to production of active oxygen species due to the presence of HAP, electrostatic interaction between HAP nanoparticles and cell wall, penetration of individual HAP nanoparticles into the cell and reformation of HAP in the entire cell [5-8]. Finally, we concluded that the antibacterial power of HAP nanoparticles may be associated with some characteristics of bacterial species [8,9].

The dependence of HAP nanoparticles on the respiration of oxygen consumed and the flow of potassium for E. coli and Bacillus sp. bacteria is listed in Table (1). It is observed that the E. coli have higher respiration of oxygen consumed and flow of potassium compared with Bacillus sp. This demonstrates that E. coli are more sensitive to HAP spherical nanoparticles than Bacillus sp. One reason for the higher respiration of oxygen consumed and flow of potassium in E. coli compared to Bacillus sp. is attributed to differences in the polarity of their cell membrane. This implies that the ability of HAP nanoparticles to inhibit growth by generation of radical oxygen species is well suggested.

Finally, the antimicrobial activity of the HAP nanoparticles compared to ampicilin, as a positive control for different bacterial species, is listed in Table (2). It can be seen in Table (2) that Gram-positive bacteria (such as Bacillus sp., Micrococcus sp., Staphylococcus aureus, Staphylococcus epiderimdis, Streptococcus pneumonia) are less susceptible to Ca ions than Gram-negative bacteria (such as Acinetobacter sp., E. coli, Klebsiella pneumonia, Proteus mirabilis, Pseudomonas aeruginosa, Salmonella sp.) due to differences in their membrane structure [1,2]. The Gram-positive bacteria have more peptidoglycan than Gram-negative bacteria because of their thicker cell wall, and because peptidoglycan are negatively charged and HAP nanoparticles are positively charged [6]. Hence, more Ca ions may get trapped by peptidoglycan in Gram-positive bacteria than in Gram-negative bacteria [4,5]. The results in Table (2) also show that the gram negative bacteria is slightly more resistant then gram positive bacteria to the action of HAP nanoparticles. The bactericidal effects of nano HAP is due to the productionof highly reactive oxygen species $\left(OH^{-}, H_2O_2 \text{ and } O_2^{2-}\right)$ on the surface of the HAP nanoparticles linked with fatal damage to the bacteria. In fact, the formation of H_2O_2 is the primary effect that contributes to the antibacterial activity, which takes place through penetration of H_2O_2 via the cell walls. Another possible explanation for the antibacterial effect is based on the abrasive surface ordering (i.e. texturing) of HAP due to surface defects and aggregates which contribute to the mechanical damage to the cell membrane of the bacteria.

IV. Conclusions

Hydroxyapatite nanoparticles was successfully synthesized via precipitation process using calcium hydroxide and orthophosphoric acid at pH 10 using NaOH for the first time. The average crystallite size of the as synthesized HAP was found to be 19 nm in size, surface area of about 61 m^2/g and crystallinity of about 87%. It is believed that the process developed in the present work is also applicable for the preparation of other hydroxyapatite-based solid-state solutions.

Antibacterial activity results show that hydroxyapatite is active against most common gram-positive and gram negative bacteria making it useful for clinical applications and environmental fields.

References

[1]. Farid El-Tantawy, Faten Al-Hazmi, Fowzia Alnowaiser, A. A. Al-Ghamdi, Attieh A. Al-Ghamdi, M.M. Aly, Reem M. Al-Tuwirqi, A new large – Scale synthesis ofmagnesium oxide nanowires:Structural and antibacterial properties, Superlattices and Microstructures, 52, 200-209, (2012).

[2]. Farid El-Tantawy, Gary W. Beall, El-Shazly M. Duraia, Faten Al-Hazmi, A. A Al-Ghamdi, Rapid fabrication of nanostructured magnesium hydroxide and hydromagnesite via microwave-assisted technique, Powder Technology, 234, 26-31, (2013).

[3]. Kaygili, C. Tatar, F. Yakuphanoglu, S. Keser, Nano-crystalline aluminum-containing hydroxyapatite based bioceramics: synthesis and characterization, J. Sol-Gel Sci Technol, 65, 105-111, (2013).

[4]. O. Kaygili, C. Tatar, The investigation of some physical properties and microstructure of Zn-doped hydroxyapatite bioceramics prepared by sol–gel method, J Sol-Gel Sci Technol, 61, 296–309, (2012).

[5]. Mehdi Sadat Shojai, Mohammad Taghi Khorasani, Ehsan Dinpanah Khoshdargi, Ahmad Jamshidi, Synthesis methods for nanosized hydroxyapatite with diverse structures, Acta Biomaterialia, 9, 7591–7621, (2013).

[6]. Shih-Ching Wu, Hsi-Kai Tsou, Hsueh-Chuan Hsu, Shih-Kuang Hsu, Shu-Ping Liou, Wen-Fu Ho, A hydrothermal synthesis of eggshell and fruit waste extract to produce nanosized hydroxyapatite, Ceramics International, 39, 8183–8188, (2013).

[7]. Gunjan Verma, K.C. Barick, N. Manoj, A.K. Sahu, P.A. Hassan, Rod-like micelle templated synthesis of porous hydroxyapatite, Ceramics International, 39, 8995–9002, (2013).

[8]. N. Neelakandeswari, G. Sangami, N. Dharmaraj, Preparation and Characterization of Nanostructured Hydroxyapatite Using a Biomaterial, Synthesis and Reactivity in Inorganic, Metal-Organic, and Nano-Metal Chemistry, 41, 513-516, (2011).

[9]. Kai Li, Sie Chin Tjong, Preparation and Characterization of Isotactic Polypropylene Reinforced with Hydroxyapatite Nanorods, Journal of Macromolecular Science, Part B: Physics, 50, 1983-1995, (2011).

[10]. L.V. Trandafilovi´c, D.K. Bo˘zani´c, S. Dimitrijevi´c-Brankovi´c, A.S. Luytc, V. Djokovi´ca, Fabrication and antibacterial properties of ZnO–alginate nanocomposites, Carbohydrate Polymers, 88, 263-269, (2012).

[11]. Reem M. Al-Tuwirqi, A.A. Al-Ghamdi, Faten Al-Hazmi, Fowzia Alnowaiser, Attieh A. Al-Ghamdi, Nadia Abdel Aal, Farid El-Tantawy, Synthesis and physical properties of mixed Co_3O_4/CoO nanorods by microwave hydrothermal technique Superlattices and Microstructures, 50, 437-448, (2011).

[12]. Ahmed A. Al-Ghamdi, Faten Al-Hazmi, R.M. Al-Tuwirqi, F. Alnowaiser, Omar A. Al-Hartomy, Farid El-Tantawy, F. Yakuphanoglu, Synthesis, magnetic and ethanol gas sensing properties of semiconducting magnetite nanoparticles, Solid State Sciences ,19, 111-116, (2013).

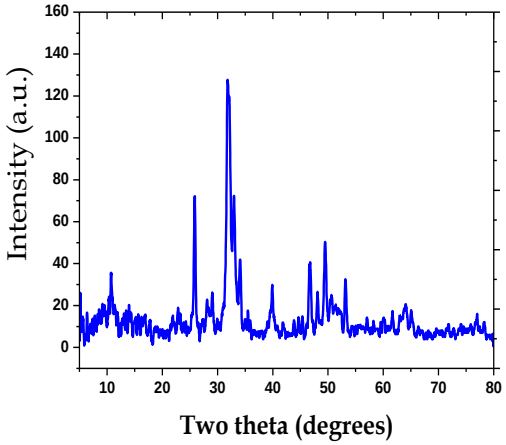

Fig. (1): X-ray pattern of the as – synthesized HAP nanoparticles.

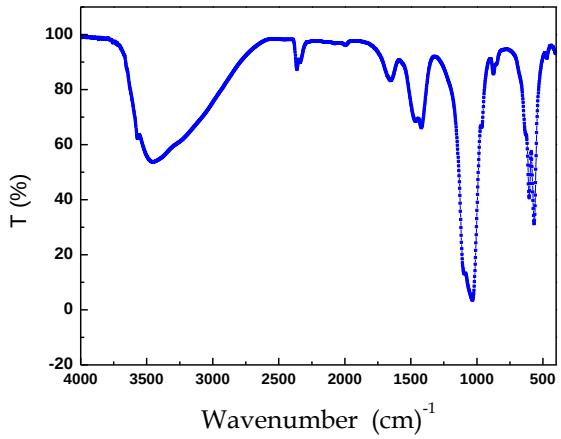

Fig. (2): FTIR pattern of the as – synthesized HAP nanoparticles.

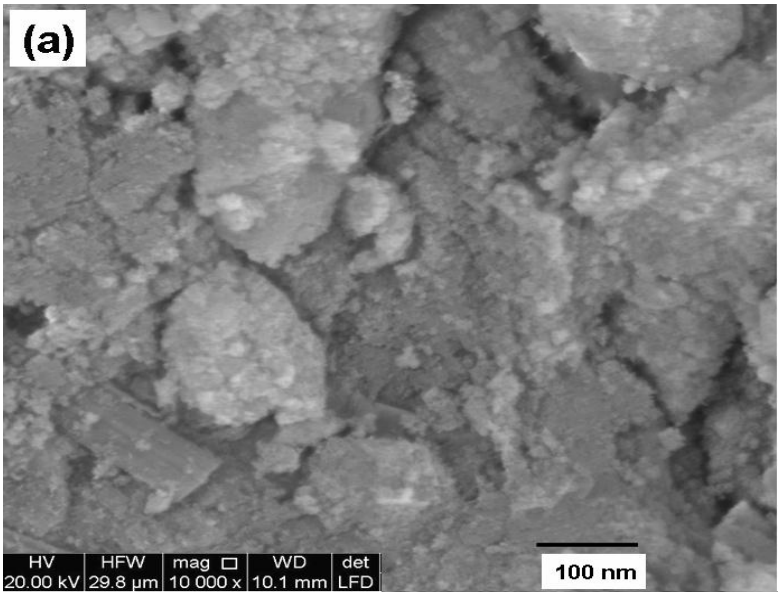

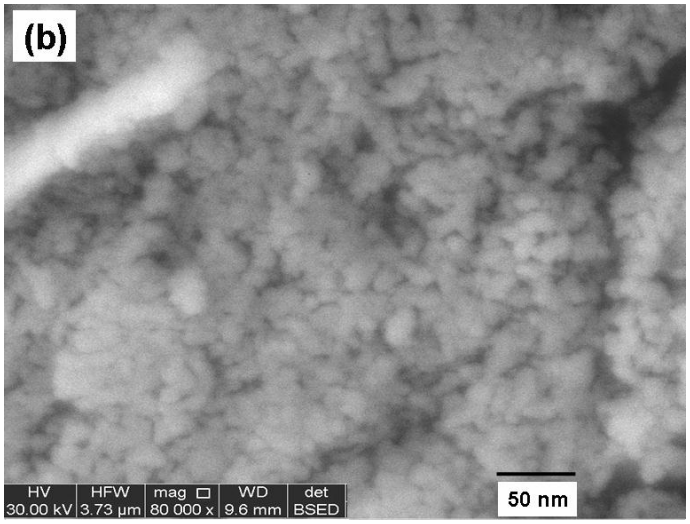

Fig. (3 a,b): SEM image of as synthesized HAP nanoparticles with different magnifications.

Element	Atomic (%)	Ca/P
O	75.76	
P	9.09	1.66
Ca	15.15	

(c)

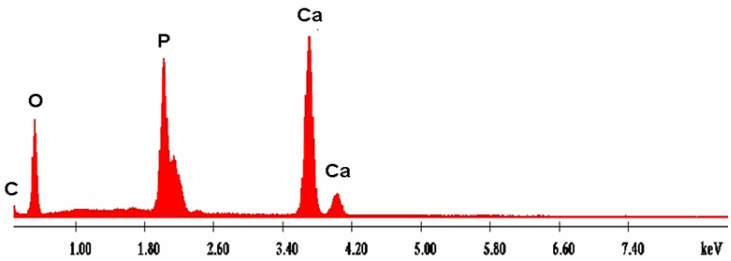

Fig. (3c): EDS analysis of HAP nanoparticles.

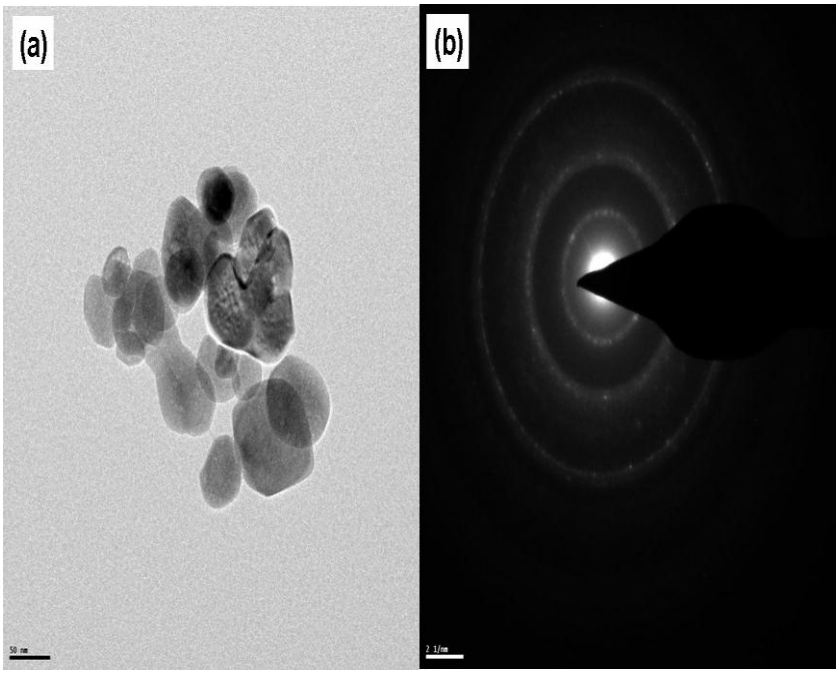

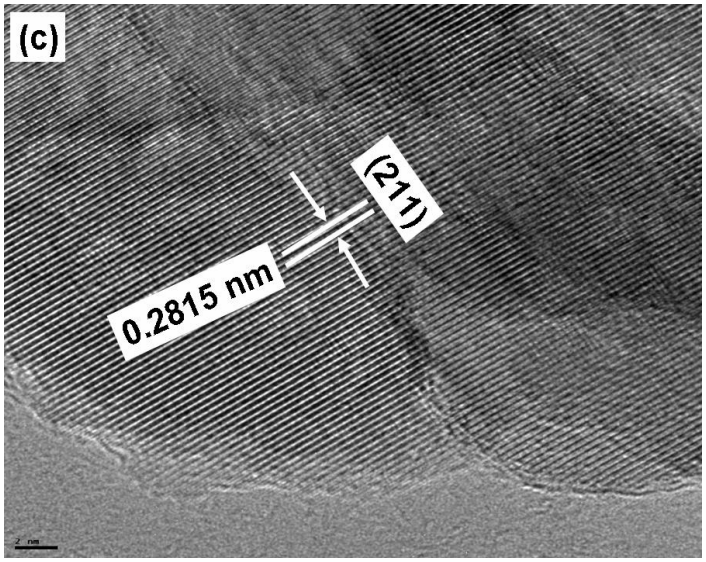

Fig. (4): (a) Low – resolution TEM of HAP nanoparticles, (b) selective area electron diffraction (SAED) and (c) High resolution TEM of HAP.

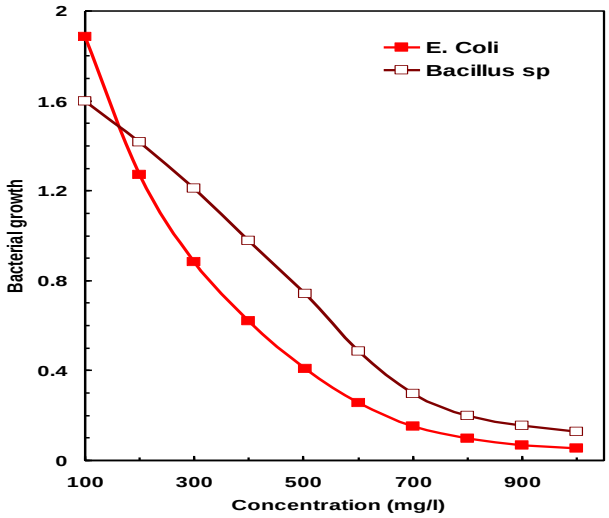

Fig. (5): Bacterial growth in liquid medium of E. coli and Bacillus sp after treatment with different concentration of HAP nanoparticles.

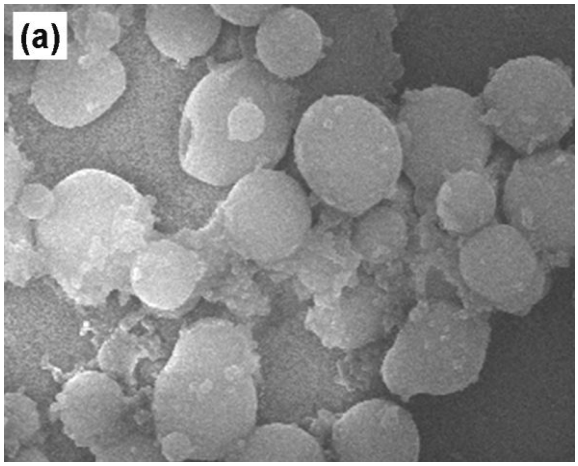

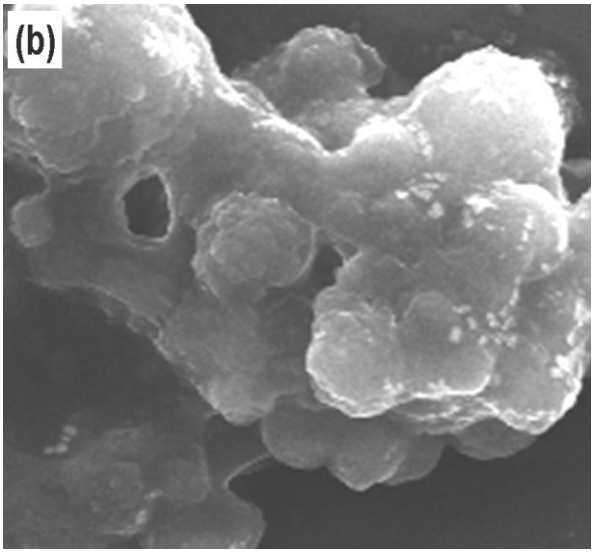

Fig. (6): (a): SEM image of normal cells of *E. coli* grown in nutrient broth medium after 24h of growth at 37°C,
(b): Treated cells of *E. coli* grown in nutrient broth medium supplemented with 0.7 g/l HAP after 24h of growth at 37°C.

Table (1): Effect of nano particles of HAP (500 µg/ml) on both respiration and flow of potassium from the plasma membranes of E. coli and Bacillus sp.

Tested bacteria	Control		HAP	
	Flow of potassium (µg /g cells)	Respiration (Quantity of O_2 consumed µmol/h.mg cells)	Flow of potassium (µg /g cells)	Respiration (Quantity of O_2 consumed µg/h.mg cells)
E. coli	14.0×10^{-7}	29.5	14.23×10^{-7}	23.4
Bacillus sp	14.0×10^{-7}	22.8	13.94×10^{-7}	20.5

Table (2): The antibacterial activity (Diameter of inhibition zone, mm) of the as prepared HAP nanoparticles compared to Ampicillin as a positive control.

Tested bacteria	Gram reaction	HAP	Positive control (Ampicillin)
Acinetobacter sp.	- ve	10.4±0. 60	15±1.0
Bacillus sp.	+ ve	13.2±0.56	30±1.5
Escherichia coli	- ve	14.9±0.97	25±4.5
Klebsiella pneumonia	- ve	8.8±0.28	24±0.5
Micrococcus spp.	+ ve	10.9±0.46	30±2.5
Proteus mirabilis	- ve	11.2±1.56	16±1.5
Pseudomonas aeruginosa	- ve	9.8±0.50	19±2.50
Salmonella sp.	- ve	10.8±4.56	20±0.56
Staphylococcus aureus	+ ve	9.0±2.56	32±0.36
Staphylococcus epiderimdis	+ ve	10.7±1.96	34±0.34

ND: + ve: Gram positive, - ve: Gram negative.